Computer Modeling in Engineering & Sciences CMES, vol.123, no.1, pp.309-332, 2020

A Comprehensive Model for Structural Non-Probabilistic Reliability and the Key Algorithms

Wencai Sun[1, *] and Zichun Yang[1]

Abstract: It is very difficult to know the exact boundaries of the variable domain for problems with small sample size, and the traditional convex set model is no longer applicable. In view of this, a novel reliability model was proposed on the basis of the fuzzy convex set (FCS) model. This new reliability model can account for different relations between the structural failure region and variable domain. Key computational algorithms were studied in detail. First, the optimization strategy for robust reliability is improved. Second, Monte Carlo algorithms (i.e., uniform sampling method) for hyper-ellipsoidal convex sets were studied in detail, and errors in previous reports were corrected. Finally, the Gauss-Legendre integral algorithm was used for calculation of the integral reliability index. Three numerical examples are presented here to illustrate the rationality and feasibility of the proposed model and its corresponding algorithms.

Keywords: Structural reliability, non-probabilistic, fuzzy convex set, robust reliability, volume ratio-based reliability, Monte Carlo, Gauss-Legendre integral formula.

1 Introduction

Engineering of practical structures involves many uncertain factors. Identifying, measuring, and controlling these uncertainties are very important for ensuring the reliability and comprehensive performance of the engineered structures. The traditional method of addressing uncertainties is based on probability theory, and its development is very mature. However, probability models depend on a large amount of objective statistical data, which are used to determine the appropriate probability density function (PDF). In practical engineering, statistical data are often insufficient due to limitations of experimental conditions and costs. In addition, some parameters, e.g., geometries, do not exhibit any randomness, and their uncertainties stem from measurement or subjective understanding of people. This is the so-called unascertained type of uncertainty [Liu, Wu and Wang (1997)]. In summary, probability theory has inherent limitations for problems with small sample size.

To overcome the limitations of probabilistic methods, Ben-Haim et al. [Ben-Haim and Elishakoff (1990)] opened a new way to deal with structural uncertainty using a non-probabilistic convex set model, which does not require a large amount of statistical

[1] Naval University of Engineering, Wuhan, 430033, China.

[*] Corresponding Author: Wencai Sun. Email: sun_wencai@163.com.

Received: 22 August 2019; Accepted: 23 October 2019.

data. Ben-Haim first proposed using a non-probabilistic concept for structural reliability [Ben-Haim (1994)] and subsequently presented a new index of non-probabilistic reliability [Ben-Haim (1995)]. Elishakoff [Elishakoff (1995)] later presented another reliability index based on the interval safety factor. Guo et al. [Guo, Lu and Feng (2001)] presented a non-probabilistic reliability model based on interval analysis and a state function describing the structural limit, and this reliability index is an infinite norm. In recent years, robust reliability theory based on convex set uncertainties has been extensively studied [Ni, Jiang and Han (2016); Yang, Zhang, Meng et al. (2017); Gou, Li, Luo et al. (2016); Liu, Yu, Li et al. (2016); Yi, Shi, Dhillon et al. (2016); Chen, Fan and Bian (2017)]. Wang et al. [Wang, Wang, Su et al. (2017)] studied the time-dependent non-probabilistic reliability problem for structures with fatigue cracks. There are many studies on non-probabilistic reliability-based optimization problems for engineering design [Meng, Hu and Zhou (2018); Meng, Zhou, Li et al. (2016); Wang, Fan and Hu (2018); Chen, Wang, Qiu et al. (2018); Hao, Wang, Liu et al. (2017); Zheng, Luo, Jiang et al. (2018); Saad, Chateauneuf and Raphael (2018)]. However, robust reliability theories are no longer applicable when the variable domain interferes with the structural failure region. Many scholars have studied the reliability problem in this case. Wang et al. [Wang, Qiu and Wu (2007)] proposed a non-probabilistic reliability model based on interval interference, and this reliability index represents the volume ratio of the safety domain to the entire variable domain. Zhou et al. [Zhou, An and An (2009)] successfully applied the volume ratio-based reliability model to reliability analysis of supercavitating bodies. Qiao et al. [Qiao, Qiu and Kong (2009)] further studied volume ratio-based reliability based on a hyper-ellipsoidal convex set model. Wang et al. [Wang, Wang, Wang et al. (2016)] studied the computational method of non-probabilistic reliability for linear structural systems. There are many other aspects of these topics. For example, Wang et al. [Wang, Zhou, Gao et al. (2018)] studied non-probabilistic sensitivity analysis and its application in optimization of aeronautical hydraulic pipelines. Fang et al. [Fang, Su, Xiao et al. (2017)] studied the non-probabilistic reliability problem for structures with an implicit performance function. Zhang et al. [Zhang, Jiang and Fang (2016)] and Khairul et al. [Khairul, Norhisham and Hong (2017)] applied non-probabilistic reliability theories to several practical engineering problems.

All the aforementioned non-probabilistic reliability methods are based on interval or hyper-ellipsoidal models, which are so-called rigid convex set models. However, when the sample size is very small, it is difficult to know the exact boundary of the variable domain. The robust reliability and volume ratio-based reliability methods cannot take into account all cases where the variable domain intersects with or is separated from the failure region, thus these methods do not have universal applicability in engineering. Sun et al. [Sun, Yang and Chen (2018)] proposed a new uncertainty model named the fuzzy convex set (FCS) model. The results presented in this paper stem from this uncertainty model. FCS has the following features: (1) the FCS model is used to establish non-probabilistic reliability model to overcome the limitations of traditional rigid convex models; (2) the new reliability model can take into account all kinds of location relationships between the failure region and the variable domain; the index is continuous, comparable, and clear in its physical meaning; (3) the location of the robust reliability index is discussed, and a previous conclusion is corrected. Then, an improved

optimization algorithm for a robust reliability index is proposed. The uniform sampling method for a hyper-ellipsoidal convex set is prepared, which revises the method in previous research reports and lays the foundation for application of volume ratio-based reliability theory. Finally, we present the numerical integration method for solving FCS-based reliability problems. All key algorithms of this new model will be presented.

2 The comprehensive structural non-probabilistic reliability model

Assume the structural limit state equation is

$$M = G(\boldsymbol{x}) = G(x_1, x_2, \cdots, x_n) = 0 \tag{1}$$

where $\boldsymbol{x}=(x_1, x_2, \cdots, x_n)$ is the uncertain variable vector. The surface $G(\boldsymbol{x})=0$ divides the variable space into two parts: the failure region Ω_f and the safe region Ω_s.

Assume the multiple FCS of the structural parameters is $\widetilde{U}(\tilde{\boldsymbol{\theta}}, \boldsymbol{\phi}, \bar{\boldsymbol{x}})$. According to **Cor**.2 in Sun et al. [Sun, Yang and Chen (2018)], the cut set of $\widetilde{U}(\tilde{\boldsymbol{\theta}}, \boldsymbol{\phi}, \bar{\boldsymbol{x}})$ under any level is certainly a convex set, and the following equation can be obtained:

$$\begin{aligned} &\widetilde{U}_\lambda(\tilde{\boldsymbol{\theta}}, \boldsymbol{\phi}, \bar{\boldsymbol{x}}) \\ &= U\left(\pi_{\tilde{\boldsymbol{\theta}}}^{-1}(\lambda), \boldsymbol{\phi}, \bar{\boldsymbol{x}}\right) \\ &= U_1\left(\pi_{\tilde{\theta}_1}^{-1}(\lambda), \phi_1, \bar{\boldsymbol{x}}_1\right) \cap U_2\left(\pi_{\tilde{\theta}_2}^{-1}(\lambda), \phi_2, \bar{\boldsymbol{x}}_2\right) \cap \cdots \cap U_k\left(\pi_{\tilde{\theta}_k}^{-1}(\lambda), \phi_k, \bar{\boldsymbol{x}}_k\right) \end{aligned} \tag{2}$$

where $\pi_{\tilde{\boldsymbol{\theta}}}^{-1}(\lambda) = \left(\pi_{\tilde{\theta}_1}^{-1}(\lambda), \pi_{\tilde{\theta}_2}^{-1}(\lambda), \cdots, \pi_{\tilde{\theta}_k}^{-1}(\lambda)\right)^{\mathrm{T}}$. Thus, the cut FCSs are completely correlated with the cut sets of the fuzzy extending parameters.

Robust reliability based on the FCS model is a fuzzy number. Assume its possibility distribution is $\pi_{\tilde{\eta}}(x)$. Corresponding to the λ-level cut set $U\left(\pi_{\tilde{\boldsymbol{\theta}}}^{-1}(\lambda), \boldsymbol{\phi}, \bar{\boldsymbol{x}}\right)$, the robust reliability index can be defined as

$$\eta(\lambda) = \pi_{\tilde{\eta}}^{-1}(\lambda) = \operatorname{sgn}\left[G(\bar{\boldsymbol{x}})\right] \max\left\{\chi \left| \left(\min_{\boldsymbol{x} \in U\left(\chi \pi_{\tilde{\boldsymbol{\theta}}}^{-1}(\lambda), \boldsymbol{\phi}, \bar{\boldsymbol{x}}\right)} \operatorname{sgn}\left[G(\bar{\boldsymbol{x}})\right] G(\boldsymbol{x}) \right) \geq 0 \right.\right\} \tag{3}$$

If $|\eta(\lambda)| \leq 1$, the convex set $U\left(\pi_{\tilde{\boldsymbol{\theta}}}^{-1}(\lambda), \boldsymbol{\phi}, \bar{\boldsymbol{u}}\right)$ interferes with the failure region Ω_f. In this case, we can define the non-probabilistic reliability index as

$$R_{\mathrm{set}}(\lambda) = \pi_{\tilde{R}_{\mathrm{set}}}^{-1}(\lambda) = \frac{V(\lambda)_{\mathrm{safe}}}{V(\lambda)_{\mathrm{all}}} \tag{4}$$

Then, the comprehensive index for non-probabilistic reliability is defined as

$$\kappa(\lambda) = \pi_{\tilde{\kappa}}^{-1}(\lambda) = \begin{cases} \eta(\lambda) & \eta(\lambda) > 1 \\ R_{\mathrm{set}}(\lambda) & |\eta(\lambda)| \leq 1 \\ \eta(\lambda) + 1 & \eta(\lambda) < -1 \end{cases}. \tag{5}$$

The reliability index defined above is based on the ordinary convex set model. Even if the nominal value point of the convex set is located in the failure region, the index is still valid. Moreover, continuity of the reliability index is guaranteed for all real numbers. The integral reliability index based on FCS is

$$R' = \int_0^1 \kappa(\lambda)\mathrm{d}\lambda = \int_0^1 \pi_{\tilde{\kappa}}^{-1}(\lambda)\mathrm{d}\lambda \tag{6}$$

When the nominal value point of the convex set is located in the failure region, and the convex set interferes with the safe region, the robust reliability index is less than 0, but the comprehensive reliability index in Eq. (5) is greater than 0. Thus, the robust reliability model cannot reasonably reflect the structural reliability in this case. This case is illustrated in Fig. 1.

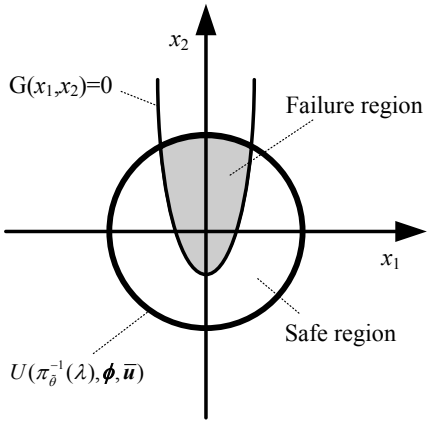

Figure 1: The case where $\eta(\lambda)<0$ and $\kappa(\lambda)>0$

Regarding the reliability problem shown in Fig.1, the robust reliability degree is $\eta(\lambda)<0$, but the comprehensive reliability index is $\kappa(\lambda)>0$. Although $\eta(\lambda)<0$ according to Fig. 1, the shaded failure region is far smaller than the safety region. Therefore, the comprehensive reliability model can more rationally measure the interference level between the failure region and the variable domain. Furthermore, the proposed integral reliability index can account for uncertainties in the structural parameters and the inaccuracy of the ordinary convex set model. Thus, this index is a more rational and comprehensive structural reliability model for problems with small sample size.

3 Key algorithms in the proposed reliability model

3.1 Normalization of the multiple convex set

The non-probabilistic reliability under any-level cut set can be obtained by spreading the original convex set or the interference between the failure region and the original convex set. However, it is often impractical to use the original convex set directly, as the designed algorithm has many difficulties. Thus, we first need to normalize the original convex set model.

Let us assume that the multiple convex set model for uncertain parameters includes p interval models and m hyper-ellipsoidal models. The interval vector $\boldsymbol{X}$ can be converted to a normalized interval variable vector with the following equation:

$$\boldsymbol{X} = \boldsymbol{X}^{\mathrm{c}} + \boldsymbol{\delta}_1 \Delta \boldsymbol{X},\ \boldsymbol{\delta}_1 \in [-1,1]^p \tag{7}$$

where, $\boldsymbol{X}^{\mathrm{c}}$ is the central vector of $\boldsymbol{X}$, $\boldsymbol{\delta}_1$ is the p-dimensional normalized interval vector, $\Delta \boldsymbol{X}$ is the deviation vector, and p denotes the dimensionality of the interval variable vector.

Let us assume that the i-th hyper-ellipsoidal model can be expressed by

$$\boldsymbol{X}_i \in \boldsymbol{E}_i\left(\boldsymbol{X}_i, \theta_i\right) = \left\{\boldsymbol{X}_i : \left(\boldsymbol{X}_i - \boldsymbol{X}_i^0\right)^{\mathrm{T}} \boldsymbol{\Omega}_i \left(\boldsymbol{X}_i - \boldsymbol{X}_i^0\right) \le \theta_i^2\right\}, i = 1,2,\cdots,m \tag{8}$$

Let us perform an eigenvalue decomposition for the positive definite matrix $\boldsymbol{\Omega}_i$:

$$\boldsymbol{\Omega}_i = \boldsymbol{Q}_i^{\mathrm{T}} \boldsymbol{D}_i \boldsymbol{Q}_i,\ \ \boldsymbol{Q}_i^{\mathrm{T}} \boldsymbol{Q}_i = \boldsymbol{I}_i \tag{9}$$

where $\boldsymbol{D}_i$ is a diagonal matrix and $\boldsymbol{I}_i$ is an identity matrix. Let us introduce the vector

$$\boldsymbol{u}_i = \left(1/\theta_i\right) \boldsymbol{D}_i^{1/2} \boldsymbol{Q}_i \boldsymbol{X}_i \tag{10}$$

According to Eq. (8), we can obtain

$$\boldsymbol{u}_i \in \left\{\boldsymbol{u}_i : \left(\boldsymbol{u}_i - \boldsymbol{u}_i^0\right)^{\mathrm{T}} \left(\boldsymbol{u}_i - \boldsymbol{u}_i^0\right) \le 1\right\}, i = 1,2,\cdots,m \tag{11}$$

or

$$\Delta \boldsymbol{u}_i \in \left\{\Delta \boldsymbol{u}_i : \Delta \boldsymbol{u}_i^{\mathrm{T}} \Delta \boldsymbol{u}_i \le 1\right\}, i = 1,2,\cdots,m \tag{12}$$

The original hyper-ellipsoidal convex set has been converted to a unit hyper-sphere through the above conversion. According to Eq. (10), we can obtain

$$\boldsymbol{X}_i = \theta_i \boldsymbol{Q}_i^{\mathrm{T}} \boldsymbol{D}_i^{-1/2} \boldsymbol{u}_i = \theta_i \boldsymbol{Q}_i^{\mathrm{T}} \boldsymbol{D}_i^{-1/2} \left(\Delta \boldsymbol{u}_i + \boldsymbol{u}_i^0\right) \tag{13}$$

After substitution of Eqs. (7) and (13) into Eq. (1), we can obtain the following normalized limit state function:

$$M = G'\left(\boldsymbol{\delta}_1, \Delta \boldsymbol{u}_1, \Delta \boldsymbol{u}_2, \cdots, \Delta \boldsymbol{u}_m\right) = 0 \tag{14}$$

To make the expression more convenient, the normalized limit state function will be written as

$$M = G'\left(\boldsymbol{\delta}\right) = G'\left(\delta_1, \delta_2, \cdots, \delta_n\right) = G'\left(\Delta \boldsymbol{u}_1, \Delta \boldsymbol{u}_2, \cdots, \Delta \boldsymbol{u}_k\right) = 0 \tag{15}$$

where n is the total number of dimensions in the non-deterministic variable space, and $\Delta \boldsymbol{u}_i$ is the normalized variable vector in the i-th submodel.

3.2 Optimization algorithm for robust reliability

3.2.1 Discussion of the robust reliability index position

Jiang et al. [Jiang and Chen (2007)] has pointed out that the robust reliability index under the interval model can only be located at one of the intersection points between the

ultra-rays (passing through the origin and the vertices of the normalized interval set) and the normalized failure surface, and a detailed proof was presented. Some applications related to this conclusion have been reported [Zhou, An and Jia (2011)].

However, the proof was not rigorous and the conclusion was somewhat biased. In order to save space, this proof will not be discussed here in detail, but the problem of the conclusion will be illustrated with a counter-example.

A 2-dimensional case is shown in Fig. 2, where the limit state surface denoted by M_1 monotonically decreases in the 2-dimensional space. The robust reliability index is indeed located at an intersection point. However, the robust reliability for M_2 is not located on the ultra-rays passing through the origin and the vertices of the interval sets. In fact, one can prove that the conclusion in Jiang et al. [Jiang and Chen (2007)] is correct if the normalized limit state surface is monotonic in the normalized interval variable space. However, when the limit state surface is not monotonic, this conclusion is not always true.

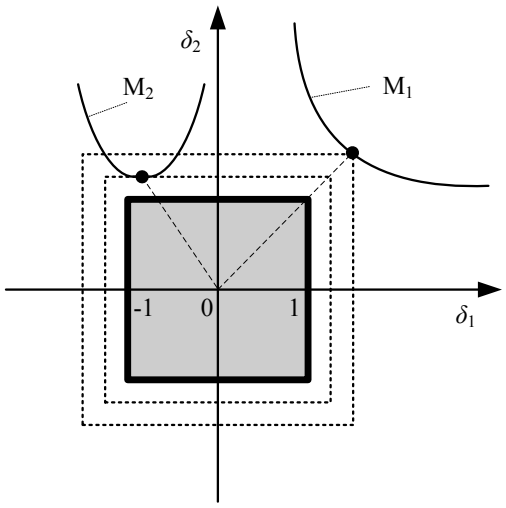

Figure 2: Location of the interval robust reliability index

When the limit state surface is monotonic, the conclusion can be proven as follows:

Proof: Assume that the n-dimensional normalized limit state surface $M=G(\delta_1,\delta_2,\ldots,\delta_n)=0$ is a monotonic surface, and the robust reliability index point is $\boldsymbol{\delta}'=\left(\delta_1',\delta_2',\cdots,\delta_n'\right)$. This conclusion will be proven by contradiction.

Assume the relation $\left|\delta_1'\right|=\left|\delta_2'\right|=\cdots=\left|\delta_n'\right|$ does not stand, and there is a relation $\left|\delta_1'\right|=\left\|\boldsymbol{\delta}'\right\|_\infty=\max\limits_{1\le i\le n}\left\{\left|\delta_i'\right|\right\}>\left|\delta_2'\right|$. Because the surface $M=0$ is monotonic, any two dimensions of this surface must be monotonic.

Case 1: Assume that $\left|\delta_1\right|$ monotonically increases with $\left|\delta_2\right|$ at the point $\boldsymbol{\delta}'=\left(\delta_1',\delta_2',\cdots,\delta_n'\right)$. Then, $\forall 0<\varepsilon<\left|\delta_2'\right|$, let $\delta_2''=\operatorname{sgn}\left(\delta_2'\right)\left(\left|\delta_2'\right|-\varepsilon\right)$ and assume the point $\boldsymbol{\delta}''=\left(\delta_1'',\delta_2'',\delta_3',\cdots,\delta_n'\right)$ is located on the normalized limit state surface $G(\boldsymbol{\delta})=0$.

We can obtain $|\delta_1''| < |\delta_1'|$, followed by $\|\boldsymbol{\delta}''\|_\infty < \|\boldsymbol{\delta}'\|_\infty$. Thus, it is impossible for $\boldsymbol{\delta}'$ to be the minimum infinite norm point, i.e., $\boldsymbol{\delta}'$ must not be the point of robust reliability.

Case 2: Assume that $|\delta_1|$ monotonically decreases with $|\delta_2|$. Then, $\forall 0 < \varepsilon < \left(|\delta_1'| - |\delta_2'|\right)$. Let $\delta_2'' = \mathrm{sgn}(\delta_2')\left(|\delta_2'| + \varepsilon\right)$ and assume that the point $\boldsymbol{\delta}'' = \left(\delta_1'', \delta_2'', \delta_3', \cdots, \delta_n'\right)$ is located on the normalized limit state surface $G(\boldsymbol{\delta})=0$. We can obtain $|\delta_1''| < |\delta_1'|$ and $|\delta_2''| = \left(|\delta_2'| + \varepsilon\right) < |\delta_1'|$, followed by $\|\boldsymbol{\delta}''\|_\infty < \|\boldsymbol{\delta}'\|_\infty$, i.e., $\boldsymbol{\delta}'$ must not be the minimum infinite norm point. In other words, it must not be the location of the robust reliability index.

In summary, $\boldsymbol{\delta}' = \left(\delta_1', \delta_2', \cdots, \delta_n'\right)$ must not be the location of the robust reliability index. Thus, $|\delta_1'| = |\delta_2'| = \cdots = |\delta_n'|$ must be true. This concludes the proof.

When the uncertain variables are described by a hyper-ellipsoidal model, the model can be converted into a unit hyper-sphere. In this hyper-sphere space, the robust reliability index point will not certainly satisfy the condition $|\delta_1'| = |\delta_2'| = \cdots = |\delta_n'|$, regardless of whether the limit state surface is monotonic or non-monotonic. As shown in Fig. 3, the limit state surface $G'(\boldsymbol{\delta})=0$ is monotonic in the normalized hyper-sphere space, but the components of the robust reliability index point are not equal.

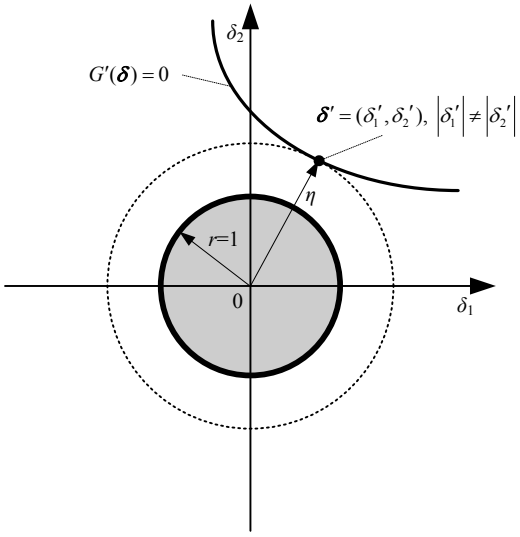

Figure 3: Location of the ellipsoidal robust reliability index

According to the above discussion, the following two corollaries can be obtained when we use a multiple convex set model to express the variables' uncertainties:

(1) When the limit state surface is monotonic in the normalized space, the following relation for the robust reliability point holds:

$$\left|\delta_1'\right| = \left|\delta_2'\right| = \left|\delta_p'\right| = \delta_{p+1}^* = \cdots = \delta_{p+m}^* \tag{16}$$

where $\delta_1', \delta_2', \cdots, \delta_p'$ are the coordinates of the p normalized interval variables and $\delta_{p+1}^*, \delta_{p+1}^*, \cdots, \delta_{p+m}^*$ are the radii of the m hyper-spheres.

(2) When the limit state surface is non-monotonic in the normalized space, any one of the following relations for the robust reliability index point may not exist:

$$\begin{cases} \left|\delta_1'\right| = \left|\delta_2'\right| = \left|\delta_p'\right| \\ \delta_{p+1}^* = \delta_{p+2}^* = \cdots = \delta_{p+m}^* \\ \left|\delta_1'\right| = \left|\delta_2'\right| = \left|\delta_p'\right| = \delta_{p+1}^* = \delta_{p+2}^* = \cdots = \delta_{p+m}^* \end{cases} \tag{17}$$

Therefore, it is very difficult to reduce the scope of the feasible solution by adding constraints when the limit state surface is non-monotonic, or if it is difficult to judge whether the surface is monotonic.

3.2.2 Improved PSO optimization strategy

In order to calculate the non-probabilistic comprehensive reliability index in Eq. (5), we first need to calculate the robust reliability index under the corresponding cut set.

According to Eq. (3), the physical meaning of $\eta(\lambda)$ is the shortest distance measured by the uncertainty level parameter χ from the centric point $\bar{\boldsymbol{x}}$ of the convex set model $U\left(\chi\pi_{\hat{\boldsymbol{\theta}}}^{-1}(\lambda), \boldsymbol{\phi}, \bar{\boldsymbol{x}}\right)$ to the failure surface $G(\boldsymbol{x})=0$. In the normalized variable space, $\eta(\lambda)$ can be obtained from the following constrained optimization problem:

$$\begin{cases} \eta(\lambda) = \operatorname{sgn}\left[G'(\mathbf{0})\right] \bullet \left|\eta(\lambda)\right| \\ \left|\eta(\lambda)\right| = \min\limits_{\boldsymbol{\delta}} \rho(\boldsymbol{\delta}) \\ \text{s.t.} \quad G'(\boldsymbol{\delta}) = 0 \end{cases} \tag{18}$$

where $\rho(\boldsymbol{\delta})$ is the distance from any point $\boldsymbol{\delta}$ to the origin derived from the normalized convex set model of the multiple convex set $U\left(\chi\pi_{\hat{\boldsymbol{\theta}}}^{-1}(\lambda), \boldsymbol{\phi}, \bar{\boldsymbol{x}}\right)$. The expression for $\rho(\boldsymbol{\delta})$ is

$$\rho(\boldsymbol{\delta}) = \max_{i=1,2,\cdots,k} \delta_i^* = \sqrt{\Delta \boldsymbol{u}_i^{\mathrm{T}} \Delta \boldsymbol{u}_i} \tag{19}$$

According to the analysis in Section 3.2.1, it is difficult to reduce the feasible region for robust reliability index when the limit state surface is not monotonic. In order to develop a universally applicable method, the algorithm for determining the robust reliability index based on particle swarm optimization (PSO) is presented here.

In this paper, the basic theory of PSO will not be thoroughly discussed. PSO is suitable for continuous and discrete functions. Li [Li (2012)] presented the following unconstrained optimization problem by introducing a penalty term:

$$\left|\eta(\lambda)\right| = \min_{\boldsymbol{\delta} \in \boldsymbol{\Omega}} \left\{ \rho(\boldsymbol{\delta}) + C_1 \Psi_1\left[G'(\boldsymbol{\delta})\right] \right\} \tag{20}$$

where

$$\Psi_1\left[G'(\boldsymbol{\delta})\right]=\begin{cases}1 & \operatorname{sgn}\left[G'(0)\right]G'(\boldsymbol{\delta})>0\\ 0 & \operatorname{sgn}\left[G'(0)\right]G'(\boldsymbol{\delta})\le 0\end{cases} \tag{21}$$

sgn (·) is sign function, and C_1 is the penalty factor. The penalty factor only needs to be greater than 10 because the non-probabilistic reliability index is usually a small number.

According to Eq. (20), the former constrained optimization problem has been converted to an unconstrained optimization problem after introducing the penalty factor. In order to improve the performance and efficiency of the PSO algorithm, another penalty factor has been introduced into the fitness function. This approach is equivalent to adding a constraint on the opposite side of the nominal value of the convex set about the limit state surface. The optimization problem remains an unconstrained problem with the following form

$$\left|\eta(\lambda)\right|=\min_{\boldsymbol{\delta}\in\Omega}\left\{\rho(\boldsymbol{\delta})+C_1\psi_1\left[G'(\boldsymbol{\delta})\right]+C_2\psi_2\left[\xi,G'(\boldsymbol{\delta})\right]\right\} \tag{22}$$

where

$$\Psi_2\left[\xi,G'(\boldsymbol{\delta})\right]=\begin{cases}1 & -\xi-\operatorname{sgn}\left[G'(\mathbf{0})\right]G'(\boldsymbol{\delta})>0\\ 0 & -\xi-\operatorname{sgn}\left[G'(\mathbf{0})\right]G'(\boldsymbol{\delta})\le 0\end{cases} \tag{23}$$

ξ is the parameter controlling the scale of the search field, and C_2 is the second penalty factor. The principle of the value of C_2 is similar to that of C_1. C_2 can meet the requirement when it is slightly larger than or equal to C_1. Because the PSO algorithm has no requirement for differentiability of the fitness function, introducing the penalty function defined in Eq. (23) is feasible and can effectively improve the efficiency of the PSO algorithm. This algorithm is shown in Fig. 4.

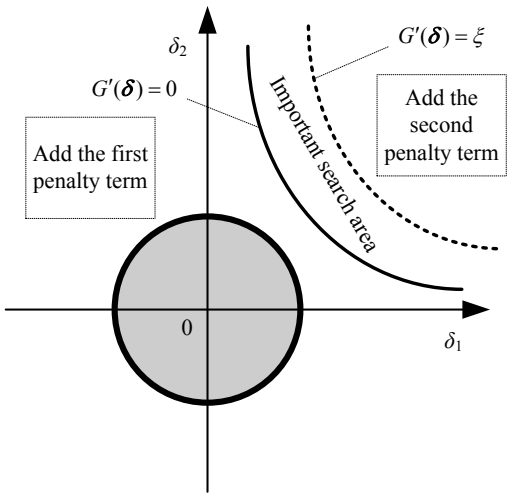

Figure 4: Schematic diagram of the PSO algorithm.

The steps of the improved PSO algorithm are as follows:

Step 1: Determine a particle's fitness function denoted by $f(\boldsymbol{\delta})$, defined as

$$f\left(\boldsymbol{\delta}\right)=\rho\left(\boldsymbol{\delta}\right)+C_1\Psi_1\left[G'\left(\boldsymbol{\delta}\right)\right]+C_2\Psi_2\left[\xi,G'\left(\boldsymbol{\delta}\right)\right] \tag{24}$$

where the values of $\boldsymbol{\delta}$ represent the location of the particles, and $\rho(\boldsymbol{\delta})$ is defined in Eq. (19). Redefine the problem as a minimization problem.

Step 2: Determine the search range and maximum velocity. According to the practical problem, make a substantial expansion of the normalized multiple convex set model and use the smallest external ultra-cuboid $\boldsymbol{I}_n=[\boldsymbol{\delta}^{\mathrm{L}},\boldsymbol{\delta}^{\mathrm{U}}]$ as the search range. In addition, define the maximum velocity as

$$\boldsymbol{v}_{\max}=0.2\times\left(\boldsymbol{\delta}^{\mathrm{U}}-\boldsymbol{\delta}^{\mathrm{L}}\right) \tag{25}$$

Step 3: Determine the parameters of the particle swarm.

Step 4: Solve by iteration. Randomly select l samples in $\boldsymbol{I}_n$ as the initial location of the particle swarm. Then, the historical best position of the particle ($\boldsymbol{\delta}_{\mathrm{b}}$), global best position ($\boldsymbol{\delta}_{\mathrm{gb}}$), and neighborhood optimum position ($\boldsymbol{\delta}_{\mathrm{nb}}$) can be obtained. The position of the next step can be determined using update formulas. Then, the values of the fitness function can be calculated, and iteration can be carried out until that the termination criteria are reached.

Step 5: Output the absolute value of the non-probabilistic reliability index, i.e., $|\eta(\lambda)|$. $|\eta(\lambda)|$ is determined from the global optimum position $\boldsymbol{\delta}_{\mathrm{gb}}$. Denote this as $\boldsymbol{\delta}_{\mathrm{gb}}=\left(\Delta\boldsymbol{u}_{1\mathrm{gb}}^{\mathrm{T}},\Delta\boldsymbol{u}_{2\mathrm{gb}}^{\mathrm{T}},\cdots,\Delta\boldsymbol{u}_{k\mathrm{gb}}^{\mathrm{T}}\right)^{\mathrm{T}}$; this yield

$$\left|\eta\left(\lambda\right)\right|=\rho\left(\boldsymbol{\delta}_{\mathrm{gb}}\right)=\max_{i=1,2,\cdots,k}\delta_i^*=\sqrt{\Delta\boldsymbol{u}_{i\mathrm{gb}}^{\mathrm{T}}\Delta\boldsymbol{u}_{i\mathrm{gb}}} \tag{26}$$

The robust reliability index can be obtained from Eq. (18). The improved PSO algorithm has better performance and efficiency. The robust reliability under any cut set level can be obtained from this algorithm and has desirable accuracy.

3.3 Monte Carlo algorithm for the hyper-ellipsoidal convex set model

According to the non-probabilistic comprehensive reliability definition in Eq. (5), the volume ratio-based reliability index $R_{\mathrm{set}}\left(\lambda\right)$ must be calculated when $\eta\left(\lambda\right)\le 1$.

In view of the difficulty involved in calculating the volumes of the structural safe or failure domains in a high dimensional ellipsoidal model and the non-linear complex limit state function, Zhou et al. [Zhou, An and Jia (2011)] presented a Monte Carlo simulation algorithm. The main procedure is: (1) convert the hyper-ellipsoidal model into hyper-sphere; (2) transform the orthogonal coordinates into spherical coordinates; (3) uniformly sample within the spherical coordinate intervals and obtain Monte Carlo samples for the hyper-sphere. Assume the dimension of the i-th hyper-sphere is n_i, its spherical coordinate is $\left(r,\theta_1,\theta_2,\cdots,\theta_{n_i-1}\right)$, and all components are intervals, i.e., $r\in[0,1]$, $\theta_1\sim\theta_{n_i-2}\in[0,\pi]$, $\theta_{n_i-1}\in[0,2\pi]$. The orthogonal coordinates and the spherical

coordinates obey the following relations:

$$\begin{cases} \Delta u_{i,1} = r\cos\theta_1 \\ \Delta u_{i,2} = r\sin\theta_1\cos\theta_2 \\ \quad\vdots \\ \Delta u_{i,n_i-1} = r\sin\theta_1\sin\theta_2\cdots\sin\theta_{n_i-2}\cos\theta_{n_i-1} \\ \Delta u_{i,n_i} = r\sin\theta_1\sin\theta_2\cdots\sin\theta_{n_i-2}\sin\theta_{n_i-1} \end{cases} \tag{27}$$

Monte Carlo samples in the orthogonal space can be obtained after performing the above transformation. However, after performing the transformation, uniform samples within the spherical coordinates will no longer follow a uniform distribution in the orthogonal space. The samples gradually become sparse as the radius increases. A 2-dimensional unit sphere with 900 samples is shown in Fig. 5, and one can find that the samples become increasingly sparse as the radius increases.

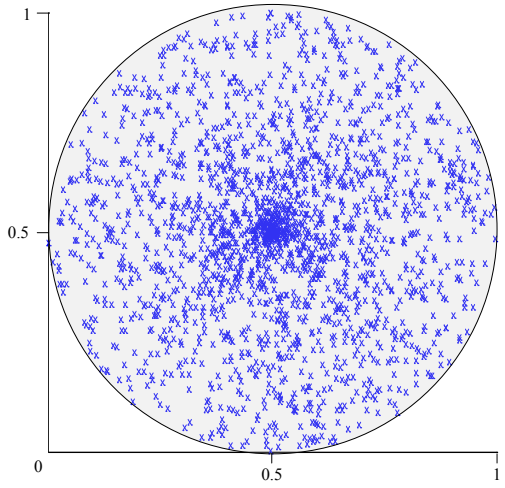

Figure 5: The distribution of samples within a unit circle

In fact, the cause of this phenomenon is not complicated. The samples are uniformly distributed along the radial direction in spherical coordinates. In other words, as long as the widths of the rings are equal, the number of samples contained in each ring tend to be equal. However, the areas of the rings increase with radius, and the samples gradually become sparse.

In order to obtain a uniform distribution of samples in a unit hyper-sphere in orthogonal coordinates, we need to change the sampling density function along the radial direction. This problem will be studied in the following section, and we will find that the density functions for hyper-spheres with different dimensions are different.

The volume of an *n*-dimensional hyper-sphere can be computed from

$$V_n = \frac{\pi^{\frac{n}{2}} R^n}{\Gamma\left(\frac{n}{2}+1\right)} = C_n R^n \tag{28}$$

where Γ is the Gamma function. $\Gamma\left(\frac{n}{2}+1\right) = \left(\frac{n}{2}\right)!$ for even n, and $\Gamma\left(\frac{n}{2}+1\right) = \sqrt{\pi}\frac{n!!}{2^{(n+1)/2}}$ for odd n. Therefore, for a given constant n, the value of C_n is

$$C_n = \begin{cases} \frac{\pi^k}{k!} & (n=2k) \\ \frac{2^{2k+1}k!\pi^k}{(2k+1)!} & (n=2k+1) \end{cases} \tag{29}$$

For an n-dimensional sphere, the area of the n-1 dimensional spherical surface is

$$S_{n-1} = \frac{dV_n}{dR} = \frac{nV_n}{R} = \frac{2\pi^{\frac{n}{2}} R^{n-1}}{\Gamma\left(\frac{n}{2}\right)} = nC_n R^{n-1} \tag{30}$$

Take two hyper ring infinitesimals at radii r_1 and r_2 with differential widths dr_1 and dr_2, respectively. The volumes of the two infinitesimals are

$$\mathrm{d}V_1 = nC_n r_1^{n-1} dr_1, \quad \mathrm{d}V_2 = nC_n r_2^{n-1} dr_2 \tag{31}$$

In order to obtain uniformly distributed samples in the orthogonal coordinates, the number of samples should be proportional to the volumes. In other words, the cumulative probabilities of r in dr_1 and dr_2 should be proportional to the volumes of the hyper rings. Denote the probability density function (PDF) along r as $f(r)$. Then we have

$$\frac{\mathrm{d}V_1}{\mathrm{d}V_2} = \frac{nC_n r_1^{n-1}\mathrm{d}r_1}{nC_n r_2^{n-1}\mathrm{d}r_2} = \frac{f(r_1)\mathrm{d}r_1}{f(r_2)\mathrm{d}r_2} \tag{32}$$

According to the above equation, we can obtain $f(r) = kr^{n-1}$. According to the properties of the PDF, we have the following if we sample randomly in a unit hyper-sphere:

$$\int_0^1 kr^{n-1}\mathrm{d}r = 1 \tag{33}$$

from which one can obtain k=n. Therefore, the PDF of r is

$$f(r) = \begin{cases} nr^{n-1} & r \in [0,1] \\ 0 & r \notin [0,1] \end{cases} \tag{34}$$

Now that we have obtained the PDF of r, generating pseudo-random numbers is another problem that must be discussed. There are only some pseudo-random number generators for typical probability distributions in common software platforms (e.g., MATLAB). For

an atypical probability distribution (e.g., $f(r)$) or even for any type of probability distribution, we need to develop additional algorithms and programs.

In this study, the required pseudo-random numbers are sampled using the Metropolis method. This method is one of the Markov chain Monte Carlo (MCMC) algorithms and can be used to draw samples from any complex distribution. The principle of Metropolis sampling is to simulate a Markov chain in a state space of random variables whose stationary distribution is the target distribution. Assuming an arbitrary distribution $f(r)$, the Metropolis sampling algorithm is as follows:

(1) At t=0, choose an initial value r_0 that meets the requirement of $f(r_0) \geq 0$.

(2) At the $(t+1)^{th}$ iteration, sample the candidate value r^c from the proposal distribution $q(r|r_t)$, which should be a symmetric distribution, such as a normal distribution or uniform distribution.

(3) Calculate $r=\min(f(r^c)/f(r_t),1)$.

(4) Construct $r_{t+1}=r^c$ with probability r, and construct $r_{t+1}=r_t$ with probability $(1-r)$.

The above sampling yields a Markov chain with stationary distribution $f(r)$, i.e., the random numbers of $f(r)$ are obtained.

Different PDFs for r should be used for hyper-spheres with different dimensions. The other components should be sampled from uniform distributions. Convert the points sampled from spherical coordinates to orthogonal coordinates, and the uniform Monte Carlo samples can be obtained.

Fig. 6 shows a 2-dimensional unit sphere including 1000 samples obtained via the modified method.

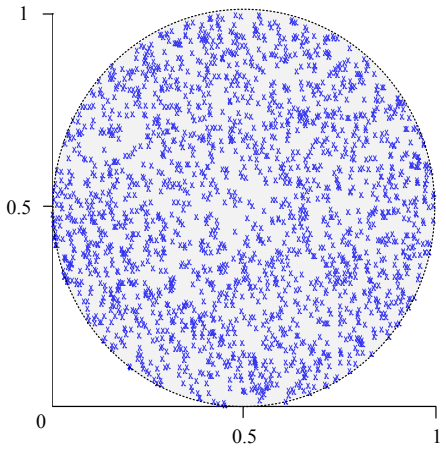

Figure 6: Distribution of samples obtained from the modified Monte Carlo algorithm

For uniform sampling of interval variables, we can use MATLAB to first degenerate the random numbers in the normalized interval variable vector $\boldsymbol{\delta}_\Delta \in [0,1]^p$. The samples in the unit interval variable vector $\boldsymbol{\delta}_1$ can be obtained from the relation $\boldsymbol{\delta}_1=2\boldsymbol{\delta}_\Delta-1$.

When the variable domain interferes with the failure region, we can use the above Monte

Carlo algorithm to calculate the non-probabilistic reliability index for a high dimensional non-linear complex limit state function as follows:

$$R_{\text{set}}(\lambda)=\lim_{q\to\infty}\frac{q_{\text{s}}}{q_{\text{all}}} \tag{35}$$

where q_{all} is the sum of all simulation calculation times, and q_{s} is the times corresponding to $G'(\boldsymbol{\delta})>0$.

3.4 Numerical integration algorithm and overall analysis procedures

In Eq. (6), the analytical form of $\kappa(\lambda)$ is difficult to obtain. Thus, it is necessary to present a numerical method to calculate the integration in Eq. (6). Given n integral nodes, the Gaussian integral formula has the highest algebraic accuracy [Yan (2006)].

Substituting $\lambda=(1+t)/2$ into Eq. (6) yields

$$R'=\int_0^1\kappa(\lambda)\mathrm{d}\lambda=\frac{1}{2}\int_{-1}^1\kappa\left(\frac{1+t}{2}\right)\mathrm{d}t \tag{36}$$

Eq. (36) can be viewed as integration from -1 to 1 with weight function $\rho(t)\equiv 1$. The corresponding orthogonal polynomials are Legendre polynomials. Thus, we can use the Gauss-Legendre integral formula to solve this problem. The Legendre polynomials are

$$L_n(t)=\frac{1}{2^n n!}\cdot\frac{\mathrm{d}^n}{\mathrm{d}t^n}\left[\left(t^2-1\right)^n\right] \tag{37}$$

Take the zero points of $L_n(t)$ as integral nodes, and the following integral formula can be obtained:

$$\int_{-1}^1 f(t)\mathrm{d}t\approx\sum_{i=1}^n A_i f(t_i) \tag{38}$$

Eq. (38) is the Gauss-Legendre integral formula. The expression for A_i is

$$A_i=\int_{-1}^1\frac{L_n(t)}{(t-t_i)L_n'(t_i)}\mathrm{d}t\quad(i=1,2,\cdots,n) \tag{39}$$

Thus, the integration in Eq. (36) can be calculated with

$$R'=\frac{1}{2}\int_{-1}^1\kappa\left(\frac{1+t}{2}\right)\mathrm{d}t\approx\frac{1}{2}\sum_{i=1}^n A_i\kappa\left(\frac{1+t_i}{2}\right) \tag{40}$$

The integral nodes and integral coefficients of Gauss-Legendre integral formula can be found in the numerical analysis monograph [Yan (2006)].

The overall analytical procedure for the proposed reliability model is as follows:

a) Build the FCS model for the structural variables, and determine the possibility distribution function for the fuzzy extending parameter.

b) n cut set levels λ_i can be obtained according to the n integral nodes t_i of the Gauss-Legendre integral formula.

c) Transform the multiple convex set models under n cut set levels into n unit convex set models, and the structural limit state function is transformed into the normalized limit state function.

d) Apply the optimization algorithm in Section 3.2 to resolve the robust reliability index $\eta(\lambda)$. If $\eta(\lambda)>1$, construct $\kappa(\lambda)=\eta(\lambda)$; if $\eta(\lambda)<-1$, construct $\kappa(\lambda)=\eta(\lambda)+1$; if $|\eta(\lambda)|\leq 1$, proceed to Step e).

e) Apply the Monte Carlo algorithm in Section 3.3 to compute the non-probabilistic reliability index $R_{\text{set}}(\lambda)$ for the case where the variable domain interferes with the failure region, and subsequently construct $\kappa(\lambda)=R_{\text{set}}(\lambda)$.

f) Calculate Eq. (40), thus yielding the final structural non-probabilistic reliability result.

4 Numerical examples and discussion

4.1 Example 1: A numerical example

Let the limit state function of a structure be

$$\begin{aligned} M = {} & X_5 - 0.00115X_1X_2 + 0.00157X_2^2 + 0.00117X_1^2 + 0.0135X_2X_3 \\ & - 0.0705X_2 - 0.00534X_1 - 0.0149X_1X_3 - 0.0611X_2X_4 \\ & + 0.0717X_1X_4 - 0.226X_3 + 0.0333X_3^2 - 0.558X_3X_4 \\ & + 0.998X_4 - 1.339X_4^2 \end{aligned}$$

where X_1-X_5 are fuzzy interval variables whose accurate boundaries cannot be obtained. Their uncertainties are described by fuzzy interval models as follows:

$$\tilde{U}_{X_1}\left(\tilde{\theta}_1,\phi_1,\overline{x}_1\right)=\left\{x\,|\,|x-10|\leq 1.5\tilde{\theta}_1\right\},\ \tilde{U}_{X_2}\left(\tilde{\theta}_2,\phi_2,\overline{x}_2\right)=\left\{x\,|\,|x-25|\leq 3\tilde{\theta}_2\right\},$$

$$\tilde{U}_{X_3}\left(\tilde{\theta}_3,\phi_3,\overline{x}_3\right)=\left\{x\,|\,|x-0.8|\leq 0.12\tilde{\theta}_3\right\},\ \tilde{U}_{X_4}\left(\tilde{\theta}_4,\phi_4,\overline{x}_4\right)=\left\{x\,|\,|x-0.0625|\leq 0.025\tilde{\theta}_4\right\},$$

$$\tilde{U}_{X_5}\left(\tilde{\theta}_5,\phi_5,\overline{x}_5\right)=\left\{x\,|\,|x-1.2|\leq 0.1\tilde{\theta}_5\right\}$$

The extending parameters $\tilde{\theta}_1$-$\tilde{\theta}_5$ follow a semi-trapezoidal distribution with small bias. The distribution functions decrease linearly from 1 to 0 and with extension parameters ranging from 1 to 1.5.

The Gauss-Legendre integral formula including seven nodes is used here. The corresponding cut set levels can be obtained from the integral nodes and the relation $\lambda=(1+t)/2$:

$$\lambda_1=0.97455395615;\lambda_2=0.02544604385;\lambda_3=0.8707655928;\lambda_4=0.1292344072;$$

$$\lambda_5=0.7029225757;\lambda_6=0.2970774243;\lambda_7=0.5$$

The integral coefficients are

$$A_1=A_2=0.1294849662;A_3=A_4=0.2797053915;A_5=A_6=0.3818300505;$$

$$A_7=0.4179591837$$

The robust reliability indices corresponding to every cut set level are

$\eta(\lambda_1)=1.1641;\eta(\lambda_2)=0.79264;\eta(\lambda_3)=1.1073;\eta(\lambda_4)=0.8213;\eta(\lambda_5)=1.0264;$
$\eta(\lambda_6)=0.8723;\eta(\lambda_7)=0.9431$

The optimization procedures for $\eta(\lambda_1)$ and $\eta(\lambda_2)$ are shown in Figs. 7 and 8.

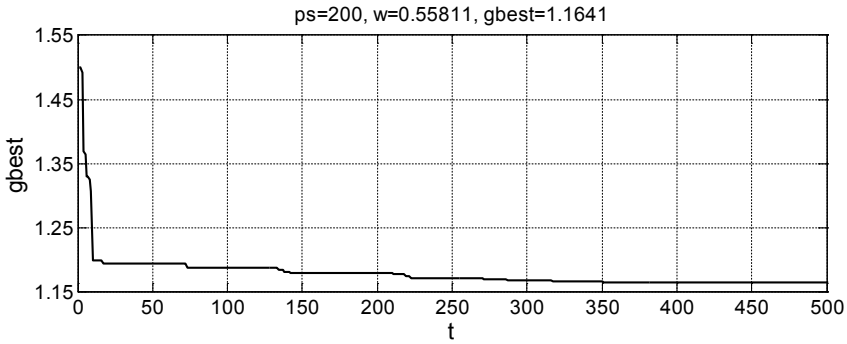

Figure 7: Optimization procedure for $\eta(\lambda_1)$

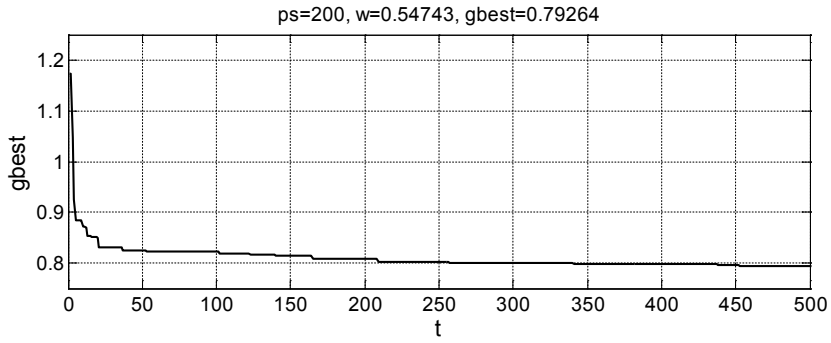

Figure 8: Optimization procedure for $\eta(\lambda_2)$

The comprehensive reliability indices corresponding to every cut set are

$\kappa(\lambda_1)=1.1641;\kappa(\lambda_2)=0.994066;\kappa(\lambda_3)=1.1073;\kappa(\lambda_4)=0.996836;$
$\kappa(\lambda_5)=1.0264;\kappa(\lambda_6)=0.9993008;\kappa(\lambda_7)=0.9999806$

The robust reliability index η and the comprehensive reliability index κ change with the cut set level, as shown in Fig. 9.

According to the Gauss-Legendre integral formula, the integral non-probabilistic reliability degree is

$$R' \approx \frac{1}{2}\sum_{i=1}^{n} A_i \kappa(\lambda_i) = 1.0297$$

If the robust reliability model is applied, the result is 0.95598.

When the cut set level is high enough, the convex set does not interfere with the failure region, and the volume-ratio based non-probabilistic reliability degree is equal to 1.

Based on this model, the integral reliability result is 0.999036.

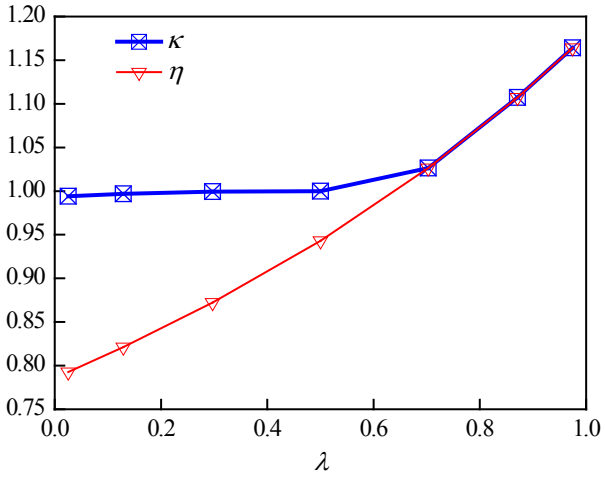

Figure 9: Variation in η and κ with λ

The difference between the results stems from the physical definitions of the various metrics. The proposed non-probabilistic reliability model takes into account the advantages of the robust reliability and volume ratio-based reliability methods. Moreover, it can account for the fuzziness of the structural parameters or the fuzziness of the ordinary convex set model. Thus, the proposed reliability model is a more comprehensive and realistic reflection of the structural reliability, but in a non-probabilistic way.

4.2 A ring-stiffened cylindrical shell example

The instability between ring ribs is one of the main failure modes of a cylindrical shell. The reliability of a ring-stiffened cylindrical shell in this failure mode will be analyzed.

The critical pressure for instability between adjacent ribs is

$$p_{cr} = C_g C_s p_E$$

where p_E denotes the Euler pressure for instability and C_g is the model correction factor that takes into account initial imperfections on the shell. C_s is the model correction factor taking into account the plastic and residual stress.

Assume the Poisson ratio of the material is 0.3, p_E can be calculated using

$$p_E = E\left(\frac{h}{r}\right)^2 \frac{0.6}{u - 0.37}$$

where E, h, and r denote the elastic modulus, thickness, and radius of the cylindrical pressure shell, respectively. u is a dimensionless parameter expressed as

$$u = 0.642l/\sqrt{rh}$$

where l is the distance between adjacent ribs.

The structural limit state equation is

$$G_{\mathrm{sh}}\left(p, p_{\mathrm{cr}}\right)=p_{\mathrm{cr}}-p=0$$

When combined with the above formulas, the limit state equation has the following form:

$$G_{\mathrm{sh}}\left(p, r, h, E, l, C_{\mathrm{s}}, C_{\mathrm{g}}\right)=C_{\mathrm{g}} C_{\mathrm{s}} E\left(\frac{h}{r}\right)^{2} \frac{0.6 \sqrt{r h}}{0.642 l-0.37 \sqrt{r h}}-p=0$$

The uncertainties in the parameters $\boldsymbol{X}=(p,\ r,\ h,\ E,\ l,\ C_{\mathrm{s}},\ C_{\mathrm{g}})^{\mathrm{T}}$ are described by the following fuzzy convex set model:

$$U_{\mathrm{E}}\left(\tilde{\theta}, 1, \overline{\boldsymbol{X}}\right)=\left\{\boldsymbol{X} \mid\left(\boldsymbol{X}-\overline{\boldsymbol{X}}\right)^{\mathrm{T}} \boldsymbol{W}_{X}\left(\boldsymbol{X}-\overline{\boldsymbol{X}}\right) \leq \tilde{\theta}^{2}\right\}$$

where $\overline{\boldsymbol{X}}=(\overline{p}, \overline{r}, \overline{h}, \overline{E}, \overline{l}, \overline{C}_{\mathrm{s}}, \overline{C}_{\mathrm{g}})^{\mathrm{T}}=(2.94, 3000, 22, 2\times10^{5}, 500, 0.9, 0.9)^{\mathrm{T}}$ and $\boldsymbol{W}_X$=Diag($1/0.15^2$, $1/180^2$, $1/1.1^2$, $1/(0.17\times10^5)^2$, $1/48^2$, $1/0.17^2$, $1/0.15^2$). $\tilde{\theta}$ follows a semi-trapezoidal distribution whose value reduces linearly from 1 to 0 and with extension parameter ranging from 1 to 2.

Here, we still use the Gauss-Legendre integral formula with seven integral nodes. The corresponding cut set levels and integral coefficients are equal to their values in Example 1.

The robust reliability values corresponding to the cut set levels are

$$\eta\left(\lambda_1\right)=1.8974; \eta\left(\lambda_2\right)=0.98536; \eta\left(\lambda_3\right)=1.7230; \eta\left(\lambda_4\right)=1.0400;$$

$$\eta\left(\lambda_5\right)=1.5000; \eta\left(\lambda_6\right)=1.1425; \eta\left(\lambda_7\right)=1.2971$$

We need to calculate the volume ratio-based non-probabilistic reliability according to the cut set level λ_2 due to $\left|\eta\left(\lambda_2\right)\right|<1$. The corresponding failure degree is 0.66×10^{-7}.

Based on the Gauss-Legendre integral formula, the integral reliability is

$$R' \approx \frac{1}{2} \sum_{i=1}^{n} A_i \kappa\left(\lambda_i\right)=1.34956$$

If the reliability analysis is based on the rigid convex set model, i.e., the kernel of the fuzzy convex set, the obtained reliability is 1.9521. It can be found that the reliability result based on the ordinary rigid convex set is higher than the value based on the FCS model. Thus, when we cannot determine the exact boundaries of the parameters, the proposed reliability model can effectively reduce the risk of the reliability analysis based on traditional rigid convex set models.

We could also use the Gauss-Legendre integral formula with more integral nodes in order to obtain higher accuracy.

4.3 A ten-bar truss example

Fig. 10 shows a ten-bar structure. There are 15 independent fuzzy interval variables, including modulus of elasticity E, rod length L, cross section areas A_i (i=1, 2,…,10), and external loads P_1, P_2, and P_3. The maximum allowable displacement in the vertical direction of node 2 is 0.06 m. The uncertainties in these variables are described using the following fuzzy interval models:

$\tilde{U}_E\left(\tilde{\theta}_E,\phi_E,\overline{x}_E\right)=\left\{x\left||x-100|\le 10\tilde{\theta}_E\right.\right\}\text{GPa}$, $\tilde{U}_L\left(\tilde{\theta}_L,\phi_L,\overline{x}_L\right)=\left\{x\left||x-1|\le 0.02\tilde{\theta}_L\right.\right\}\text{m}$,

$\tilde{U}_{P_1}\left(\tilde{\theta}_{P_1},\phi_{P_1},\overline{x}_{P_1}\right)=\left\{x\left||x-800|\le 100\tilde{\theta}_{P_1}\right.\right\}\text{kN}$, $\tilde{U}_{P_2}\left(\tilde{\theta}_{P_2},\phi_{P_2},\overline{x}_{P_2}\right)=\left\{x\left||x-100|\le 15\tilde{\theta}_{P_2}\right.\right\}\text{kN}$,

$\tilde{U}_{P_3}\left(\tilde{\theta}_{P_3},\phi_{P_3},\overline{x}_{P_3}\right)=\left\{x\left||x-100|\le 15\tilde{\theta}_{P_3}\right.\right\}\text{kN}$,

$\tilde{U}_{A_1\sim A_{10}}\left(\tilde{\theta}_{A_1\sim A_{10}},\phi_{A_1\sim A_{10}},\overline{x}_{A_1\sim A_{10}}\right)=\left\{x\left||x-0.001|\le 0.0001\tilde{\theta}_{A_1\sim A_{10}}\right.\right\}\text{m}^2$

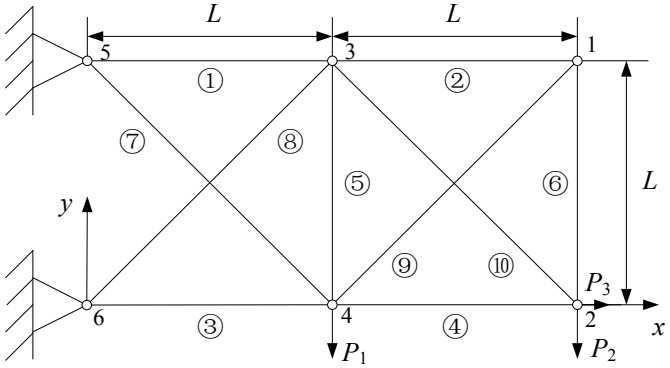

Figure 10: Ten-bar truss structure

The vertical displacement function of node 2 is

$$y_2(x)=\left(\sum_{i=1}^{6}\frac{N_i^0N_i}{A_i}+\sqrt{2}\sum_{i=7}^{10}\frac{N_i^0N_i}{A_i}\right)\frac{L}{E}$$

where N_i is the axial force in every member, N_i^0 represents the axial force when P_1=P_3=0, and P_2=1N. N_i can be easily obtained as follows:

$$N_1=P_2-\frac{\sqrt{2}}{2}N_8,\quad N_2=-\frac{\sqrt{2}}{2}N_9,\quad N_3=-P_1-2P_2+P_3-\frac{\sqrt{2}}{2}N_8$$

$$N_4=-P_2+P_3-\frac{\sqrt{2}}{2}N_9,\quad N_5=-P_2-\frac{\sqrt{2}}{2}N_8-\frac{\sqrt{2}}{2}N_9,\quad N_6=-\frac{\sqrt{2}}{2}N_9,$$

$$N_7=\sqrt{2}\left(P_1+P_2\right)+N_8,\quad N_8=\frac{a_{22}b_1-a_{12}b_2}{a_{11}a_{22}-a_{12}a_{21}},\quad N_9=\frac{a_{11}b_2-a_{21}b_1}{a_{11}a_{22}-a_{12}a_{21}},\quad N_{10}=\sqrt{2}P_2+N_9$$

where

$$a_{11}=\left(\frac{1}{A_1}+\frac{1}{A_3}+\frac{1}{A_5}+\frac{2\sqrt{2}}{A_7}+\frac{2\sqrt{2}}{A_8}\right)\frac{L}{2E},\quad a_{22}=\left(\frac{1}{A_2}+\frac{1}{A_4}+\frac{1}{A_5}+\frac{1}{A_6}+\frac{2\sqrt{2}}{A_9}+\frac{2\sqrt{2}}{A_{10}}\right)\frac{L}{2E},$$

$$a_{12}=a_{21}=\frac{L}{2A_5E},\quad b_1=\left(\frac{P_2}{A_1}-\frac{2P_2+P_1-P_3}{A_3}-\frac{P_2}{A_5}-\frac{2\sqrt{2}\left(P_1+P_2\right)}{A_7}\right)\frac{\sqrt{2}L}{2E},$$

$$b_2 = \left(\frac{\sqrt{2}\left(P_3 - P_2\right)}{A_4} - \frac{\sqrt{2}P_2}{A_5} - \frac{4P_2}{A_{10}} \right) \frac{L}{2E}$$

Here, we still use the Gauss-Legendre integral formula with seven integral nodes. The corresponding cut set levels and integral coefficients are equal to their values in Example 1.

The robust reliability index η and the comprehensive reliability index κ both change with the cut set level, as shown in Fig. 11.

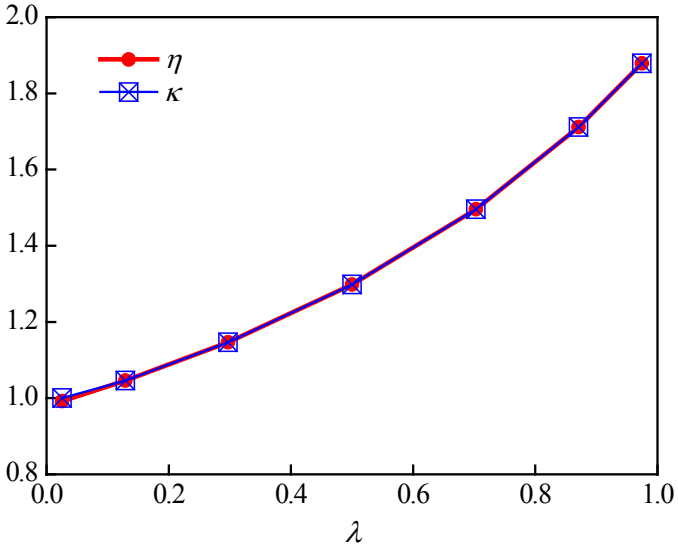

Figure 11: Variation in η and κ with λ

According to the Gauss-Legendre integral formula, the integral non-probabilistic reliability degree is

$$R' \approx \frac{1}{2}\sum_{i=1}^{n} A_i \kappa\left(\lambda_i\right) = 1.3478$$

If the reliability analysis is based on the kernel of the fuzzy convex sets which are traditional rigid convex set models, the obtained reliability is 1.9237, which is obviously higher than the result based on the FCS model. As discussed in Section 4.2, when statistical samples of parameters are scarce, the exact boundaries of these parameters cannot be determined accurately. In this case, the proposed reliability model based on FCS model can better reflect the actual engineering, and effectively reduce the risk of the reliability analysis based on traditional rigid convex set models.

Here, we offer the following discussion:

(1) When the structural failure region and the variable domain do not intersect, the volume ratio-based non-probabilistic reliability index is equal to 1. When the two regions interfere, the robust reliability index cannot strictly reflect the relationship or comparison between the failure and safety domains. The proposed reliability model in this paper is a comprehensive index, which can overcome the above two problems, and it is more

reasonable and scientific. In addition, the new index is smooth, continuous, comparable, and has a clear physical definition.

(2) For problems with small sample size, the traditional rigid convex model cannot strictly express the structural uncertainties, i.e., the boundaries of the variable domain are difficult to determine. The FCS model can take into account fuzzy boundary information. Therefore, the proposed reliability model based on FCS can take into account different position relations between the variable domain and the failure region, as well as the uncertain information regarding the variable boundaries.

(3) The examples demonstrated the correctness and effectiveness of the presented algorithms in the proposed non-probabilistic reliability theory. The improved optimization strategy based on PSO is especially suited for high dimensional reliability problems and has high efficiency. The amended Monte Carlo method for the hyper ellipsoidal model (i.e., the uniform sampling algorithm) provides corrections for errors that were previously reported in the literature. The pseudorandom number sampling method based on the Metropolis method for the PDF of r is very clever and scientific. The numerical integral algorithm based on the Gauss-Legendre integral formula is suitable for use in the proposed reliability model, and the accuracy increases with the number of integration points.

5 Conclusions

In this paper, a comprehensive reliability model was presented based on a fuzzy convex set model, and the key computational algorithms were studied in detail. The proposed reliability model can account for the various position relations between the structural failure region and the variable domain, and the index has a better physical meaning. It is smooth, continuous, and comparable. In addition, this novel model can overcome the limitations of the traditional rigid convex set model, especially for problems with small sample size. The improved optimization strategy ensures the robust reliability computation is efficient and accurate. The uniform sampling strategy for use in the hyper ellipsoidal model and the pseudorandom number simulation method for an atypical probability distribution function lays the foundation for the volume ratio-based reliability analysis. Integration of the comprehensive reliability index with the cut set level was solved with the Gauss-Legendre integral formula. The correctness and efficiency of the novel reliability model and all of the presented algorithms were demonstrated by applying them to three numerical examples.

Although this study focuses on structural reliability problems, some of the presented methods can be extended to other engineering fields, such as structural static and dynamic responses, structural fatigue prediction, buckling and post buckling, etc. These areas are interesting for future studies.

Acknowledgement： This work is funded by National Natural Science Foundation of China (No. 51509254).

Conflicts of Interest: The authors declare that they have no conflicts of interest to report

regarding the present study.

References

Ben-Haim, Y. (1994): A non-probabilistic concept of reliability. *Structural Safety*, vol. 14, no. 4, pp. 227-245.

Ben-Haim, Y. (1995): A non-probabilistic measure of reliability of linear systems based on expansion of convex models. *Structural Safety*, vol. 15, no. 2, pp. 91-109.

Ben-Haim, Y.; Elishakoff, I. (1990): *Convex Models of Uncertainty in Applied Mechanics*. Elsevier Science Publishers.

Chen, X.; Wang, X. J.; Qiu, Z. P.; Wang, L.; Li, X. et al. (2018): A novel reliability-based two-level optimization method for composite laminated structures. *Composite Structures*, vol. 192, pp. 336-346.

Chen, X. Y.; Fan, J. P.; Bian, X. Y. (2017): Theoretical analysis of non-probabilistic reliability based on interval model. *Acta Mechanica Solida Sinica*, vol. 30, no. 6, pp. 638-646.

Elishakoff, I. (1995): Discussion on: a non-probabilistic concept of reliability. *Structural Safety*, vol. 17, no. 3, pp. 195-199.

Fang, Y. B.; Su, Y. H.; Xiao, W.; Liang, B. (2017): Non-probabilistic reliability model for implicit performance function based on subinterval method. *Rock and Soil Mechanics*, vol. 38, no. 4, pp. 1171-1179.

Gou, X. W.; Li, A. J.; Luo, L. Q.; Wang, C. Q. (2016): A new method for structural non-probabilistic reliability analysis based on interval analysis. *Multidiscipline Modeling in Materials and Structures*, vol. 12, no. 1, pp. 73-79.

Guo, S. X.; Lu, Z. Z.; Feng, Y. S. (2001): A non-probabilistic model of structural reliability based on interval analysis. *Chinese Journal of Computational Mechanics*, vol. 18, no. 1, pp. 56-60.

Hao, P.; Wang, Y. T.; Liu, X. X.; Wang, B.; Li, G. et al. (2017): An efficient adaptive-loop method for non-probabilistic reliability-based design optimization. *Computer Methods in Applied Mechanics and Engineering*, vol. 324, pp. 689-711.

Jiang, T.; Chen, J. J. (2007): A semi-analytic method for calculating non-probabilistic reliability index based on interval models. *Applied Mathematical Modelling*, vol. 31, no. 7, pp. 1362-1370.

Khairul, H. P.; Norhisham, B.; Hong, H. (2017): The use of a non-probabilistic artificial neural network to consider uncertainties in vibration-based-damage detection. *Mechanical Systems and Signal Processing*, vol. 83, pp. 194-209.

Li, K. F. (2012): *Study on the Non-probabilistic Reliability Methods for Structures based on Info-gap Theory (Ph.D. Thesis)*. Naval University of Engineering, Wuhan.

Liu, K. D.; Wu, H. Q.; Wang, N. P. (1997): *Unascertained Mathematics*. Press of Huazhong University of Science and Technology.

Liu, Z.; Yu, L.; Li, Y. F.; Mi, J.; Huang, H. Z. (2016): Comparisons of two non-probabilistic structural reliability analysis methods for Aero-engine. *International*

Journal of Turbo and Jet Engines, vol. 34, no. 3, pp. 295-303.

Meng, Z.; Hu, H.; Zhou, H. L. (2018): Super parametric convex model and its application for non-probabilistic reliability-based design optimization. *Applied Mathematical Modelling*, vol. 55, pp. 354-370.

Meng, Z.; Zhou, H. L.; Li, G.; Yang, D. (2016): A decoupled approach for non-probabilistic reliability-based design optimization. *Computers and Structures*, vol. 175, pp. 65-73.

Ni, B. Y.; Jiang, C.; Han, X. (2016): An improved multidimensional parallelepiped non-probabilistic model for structural uncertainty analysis. *Applied Mathematical Modelling*, vol. 40, pp. 4727-4745.

Qiao, X. Z.; Qiu, Y. Y.; Kong, X. G. (2009): A non-probabilistic model of structural reliability based on ellipsoidal convex model. *Engineering Mechanics*, vol. 26, no. 11, pp. 203-208.

Saad, L.; Chateauneuf, A.; Raphael, W. (2018): Robust formulation for reliability-based design optimization of structures. *Structural & Multidisciplinary Optimization*, vol. 57, no. 6, pp. 2233-2248.

Sun, W. C.; Yang, Z. C.; Chen, G. B. (2018): Structural eigenvalue analysis under the constraint of fuzzy convex set model. *Acta Mechanica Sinica*, vol. 34, no. 4, pp. 653-666.

Wang, L.; Wang, X. J.; Su, H.; Lin, G. (2017): Reliability estimation of fatigue crack growth prediction via limited measured data. *International Journal of Mechanical Sciences*, vol. 121, pp. 44-57.

Wang, M. R.; Fan, J. P.; Hu, J. (2018): A non-probabilistic reliability-based design optimization method for structures based on interval models. *Fatigue & Fracture of Engineering Materials & Structures*, vol. 41, no. 2, pp. 425-439.

Wang, R. X.; Wang, X. J.; Wang, L.; Chen, X. (2016): Efficient Computational Method for the Non-Probabilistic Reliability of Linear Structural Systems. *Acta Mechanica Solida Sinica*, vol. 29, no. 3, pp. 284-299.

Wang, W. X.; Zhou, C. C.; Gao, H. S.; Zhang, Z. (2018): Application of non-probabilistic sensitivity analysis in the optimization of aeronautical hydraulic pipelines. *Structural & Multidisciplinary Optimization*, vol. 57, no. 6, pp. 2177-2191.

Wang, X. J.; Qiu, Z. P.; Wu, Z. (2007): Non-probabilistic set-based model for structural reliability. *Acta Mechanica Sinica*, vol. 39, no. 5, pp. 641-646.

Yan, Q. J. (2006): *Numerical Analysis.* Press of Beijing University of Aeronautics and Astronautics.

Yang, Z. M.; Zhang, Y. J.; Meng, W. J.; Cai, J. (2017): A convex model approach for structure non-probabilistic reliability analysis. *Journal of Risk and Reliability*, vol. 231, no. 5, pp. 508-515.

Yi, X. J.; Shi, J.; Dhillon, B. S.; Dong, H. P.; Lai, Y. H. (2016): Reliability prediction approach based on non-probabilistic interval analysis: case study of transmission system. *Proceedings of the ASME 2016 International Mechanical Engineering Congress and Exposition*.

Zhang, Y. W, Jiang, G. Q.; Fang, B. (2016): Suppression of panel flutter of near-space aircraft based on non-probabilistic reliability theory. *Advances in Mechanical Engineering*, vol. 8, no. 3, pp. 1-12.

Zheng, J.; Luo, Z.; Jiang, C.; Ni, B.; Wu, J. (2018): Non-probabilistic reliability-based topology optimization with multidimensional parallelepiped convex model. *Structural & Multidisciplinary Optimization*, vol. 57, no. 6, pp. 2205-2221.

Zhou, L.; An, W. G.; An, H. (2009): Non-probabilistic reliability analysis of supercavitating vehicles based on structure strength and buckling. *Journal of Harbin Engineering University*, vol. 30, no. 4, pp. 362-367.

Zhou, L.; An, W. G.; Jia, H. G. (2011): Definition and solution of reliability comprehensive index of super-ellipsoid convex set. *Acta Aeronautica et Astronautica Sinica*, vol. 32, no. 11, pp. 2025-2035.